



TECHNICAL ARTICLE

Preparation, Wear Resistance, and Corrosion Performance of Arc-Sprayed Zn, Al, and Zn-Al Coatings on Carbon Steel Substrates

Wangping Wu, Guoqing Sun, Qinqin Wang, and Sheng Lin

Submitted: 7 November 2022 / Revised: 26 December 2022 / Accepted: 6 January 2023 / Published online: 6 February 2023

Zn-Al coatings have attention to corrosion resistance in marine environments. In this study, Zn and Al single coatings, and Zn-Al mixed coating were obtained by an arc spray technique on carbon steel substrates. Zn and Al coatings comprised single Zn and Al phases, and some oxides. Zn-Al coating was composed of 46 at.% Al, 53 at.% Zn, and a few of oxygen. Zn-Al coating was a pseudo-alloy coating mechanically mixed with Zn, Al, and alloy phases. The cross-sectional microhardness values of Zn, Al, and Zn-Al coatings were 173.8 HV_{0.5}, 181.69 HV_{0.5}, and 259.88 HV_{0.5}, respectively. The friction coefficients of Al, Zn, and Zn-Al coatings were 0.7, 0.55, and 0.5, respectively. The wear and corrosion resistances of Zn-Al coating were better compared with single metallic coatings. The corrosion mechanisms of single Zn, Al coatings, and Zn-Al coatings were addressed and studied. Zn-Al coating could offer better wear resistance and anticorrosion performance for marine engineering steel, compared with Zn and Al coatings.

Keywords arc spraying, coating, corrosion, Zn-Al

1. Introduction

Corrosion is one of the key concerns in modern industries, especially marine, petrochemicals, and city building, which further influences the service reliability and health of components. Cost-effective steel metals are widely used for constructing marine structures (Ref 1). Steel constructions and components encounter severe corrosion damage in the corrosion environments (Ref 2-5). The coating could be the most effective approach for relieving and inhibiting corrosion, to prolong the service life of the steel components. The thermal spray technique is an efficient surface protection approach, which could fabricate protective coatings (Ref 6-9). Thermally sprayed Al-Cu and Zn-Al coatings have been used for offshore steel structures (Ref 10). Arc spraying is a thermal spray process in which an electric arc is struck between two consumable electrodes, and the compressed gas is used to atomize and propel the melted electrode materials to the substrate. Wire-arc spraying technique is widely used, due to some advantages, including economical energy saving and high efficiency (Ref 11-14), which is a cost-effective way to produce a protective layer on the surface of steel components.

Wangping Wu, Guoqing Sun, and Sheng Lin, Electrochemistry and Corrosion Laboratory, School of Mechanical Engineering and Rail Transit, Changzhou University, Changzhou 213164, People's Republic of China; Qinqin Wang, School of Mechanical Engineering, Yangzhou University, Yangzhou 225127, People's Republic of China. Contact e-mails: wwp3.14@163.com and wuwping@cczu.edu.cn.

Al and Zn coatings have good anti-corrosion and low cost, which have been extensively used in industrial applications to protect steel components against corrosion. The arc-sprayed Al and Zn single coatings and Zn-Al coatings have positive performance in the protection of the components in the corrosion environments (Ref 15, 16), or the marine environment containing chloride ions (Ref 17-20). Santos et al. (Ref 21) studied the corrosion resistance of Zn-based coatings on interstitial free steels and found Zn55Al coating had homogeneous corrosion and an effective barrier effect. The corrosion resistance of arc-sprayed Zn-Al coating was better than that of Zn and Al coatings, because the corrosion products (Ref 22), and the formation of alloying Al with Zn coating could enhance the anti-corrosion performance of Zn-Al coating (Ref 22-26).

To date, researchers focus on the fabrication and anti-corrosion performance of Zn-Al coatings in the marine environment containing Cl⁻ ion (Ref 27-33). Zn-Al coating shows higher corrosion resistance to the seawater than Zn and Al coatings. Kim and Lee (Ref 32) studied the corrosion resistance of arc-sprayed Zn-Al coatings in the marine environment and showed ZnO and Zn₅(OH)₈Cl₂·H₂O corrosion products were formed, which could improve the corrosion resistance of the base material. Zhu et al. (Ref 34) studied the influence of Al-content on the corrosion behavior of arc-sprayed Zn-Al coatings and found that as the immersion time increased, the corrosion potential and current values of Zn-15.9Al and Zn-21.1Al coatings fluctuated to some degree, while for Zn-30.1Al coating, the corrosion potential increased and the corrosion current decreased, exhibiting high corrosion resistance. Lin and Li (Ref 35) reported the corrosion behavior of arc-sprayed Zn and Zn15Al coatings on the steel in the corrosive solution and concluded that the anti-corrosion performance of the steel was significantly improved by the coatings.

The anti-corrosion performance of Zn-Al coating has been studied in the published literatures (Ref 36, 37). However, few

reports have studied the mechanical properties and wear resistance of Zn-Al coating. The arc-sprayed Zn-Al coating can effectively enhance the anti-slip coefficient of the contact surfaces and has good wear resistance. Chen et al. (Ref 38) studied the wear behavior of thermally sprayed Al, Zn-15Al, and Inconel 625 coatings and found Inconel 625 coating had higher wear resistance compared with the other coatings. Darabi and Azarmi (Ref 39) investigated the dependence of hardness on the microstructure of arc-sprayed Zn-Al coatings and found the splat boundaries resulted in the reduction in hardness of the coatings, consequently, lower elastic modulus of the wire-arc-sprayed Zn-15Al coating in the longitudinal direction compared to the transversal one.

In this study, Zn-Al coating was sprayed by wire arc spraying technique. The surface topography, microstructure, phase identification, chemical composition, microhardness, wear, and corrosion resistance of Zn-Al coating were studied in detail, at the same time compared with single metallic coatings of Zn and Al.

2. Experimental

2.1 Preparation

Q235 low-carbon steel plates (Size: 200 mm × 100 mm × 3 mm) were selected as the substrate. The chemical composition of the substrate is shown in Table 1. Before arc spraying, the sandblasting process was adopted to remove impurities on the substrate and to enhance the surface roughness. Using Zn and Al wires, the coatings were sprayed on the steel base by an industrial twin-wire arc spraying system device ((ARC 9000) from TAFE (Concord city, USA)). Table 2 displays the deposition parameters of the arc spraying process. The deposition parameters of arc-sprayed coatings were the same, the voltage of 30 V, the applied current of 200A, the distance between the base and the spraying nozzle of 150 mm, and the compressed air pressure of 0.8 MPa.

Table 1 Chemical composition of the Q235 low-carbon steel (mass fraction, wt.%)

C	Mn	Si	S	P	Fe
0.20	1.4	0.35	0.045	0.045	97.96

Table 2 Arc spraying process parameters for the coatings

Coatings	Zn	Al	Zn-Al
Spray voltage, V	30	30	30
Spray current, A	200	200	200
Spray angle, °	90	90	90
Spray distance, mm	150	150	150
Atomized gas pressure, Mpa	0.8	0.8	0.8
Spray gun movement speed, mm/s	200	200	200

2.2 Characterizations

Some small-size specimens (Size: 15 × 15 × 3 mm) were cut by an NC wire EDM machine. The cross section of the specimen was ground and polished with metallographic sandpaper (5–20 μm), and finally polished with a 1 μm diamond solution. The microstructure and chemical composition of the coatings were observed by scanning electron microscopy (Sigma 500, ZEISS, Oberkochen, DE) attached energy-dispersive spectroscopy (EDS), and an optical microscope equipped with an ultra-depth-of-field 3D microscope system (VHX-700FC, KEYENCE, Osaka, JP). The phase and crystal structure of the coatings were characterized by x-ray diffractometers (XRD, D-MAX 2500, Rigaku, Tokyo, JP).

2.3 Microhardness

The microhardness of the coating was carried out by image analysis microhardness tester (HMV-2000, SHIMADZU, Kyoto-fu, JP) under the load of 5N, and a holding time of 15 s. The final value was averaged by five indentations. The porosity of the coating was analyzed by Image J software.

2.4 Abrasion Resistance

The anti-wear performance of the coating was assessed by a material surface property comprehensive tester (CFT-1, Zhongke Kaihua, Lanzhou, CN), under the load of 2N, grinding ball material of Si₃N₄, the reciprocating stroke of 10 mm, friction speed of 400 r min⁻¹ for 15 min. The morphology and depth of the wear scratches were imaged by an optical microscope equipped with an ultra-depth-of-field 3D microscope system (VHX-700FC).

2.5 Corrosion Resistance

The corrosion resistance of the coatings was studied by an electrochemical workstation (CHI660E, Chenhua, Shanghai, CN). The coating on the substrate as the working electrode adhered to a copper conductive wire, and then manually coated with epoxy resin, leaving a geometrical surface area of 1 cm² exposed to 3.5 wt.% NaCl solution. There was a three-compartment electrode, an Ag/AgCl 3 M KCl as the reference electrode, and a Pt electrode (size: 15 × 15 × 0.5 mm) as the counter electrode. Firstly, the steady-state open circuit potential (OCP) was tested for 400 s. Subsequently, the electrochemical impedance spectroscopic (EIS) was measured at the frequency of 0.01 ~ 10⁵ Hz. Lastly, the dynamic polarization was measured at a sweep rate of 10 mV s⁻¹.

3. Results and Discussion

3.1 Characterization

The optical micrographs of the top-surface morphology of the coatings are shown in Fig. 1. In Fig. 1(a), Zn coating was smooth and flat. In addition, the coating was uniform and consistent, with no evidence of cracks and bulges. Because Zn has a low melting point of 419.53 °C, Zn wire can be fully melted during the spraying process, the atomization effect was better than that of Al wire. In Fig. 1(b), Al coating was off-white and bright color, the surface is rough, and there were no obvious defects. Because Al has a relatively high melting point

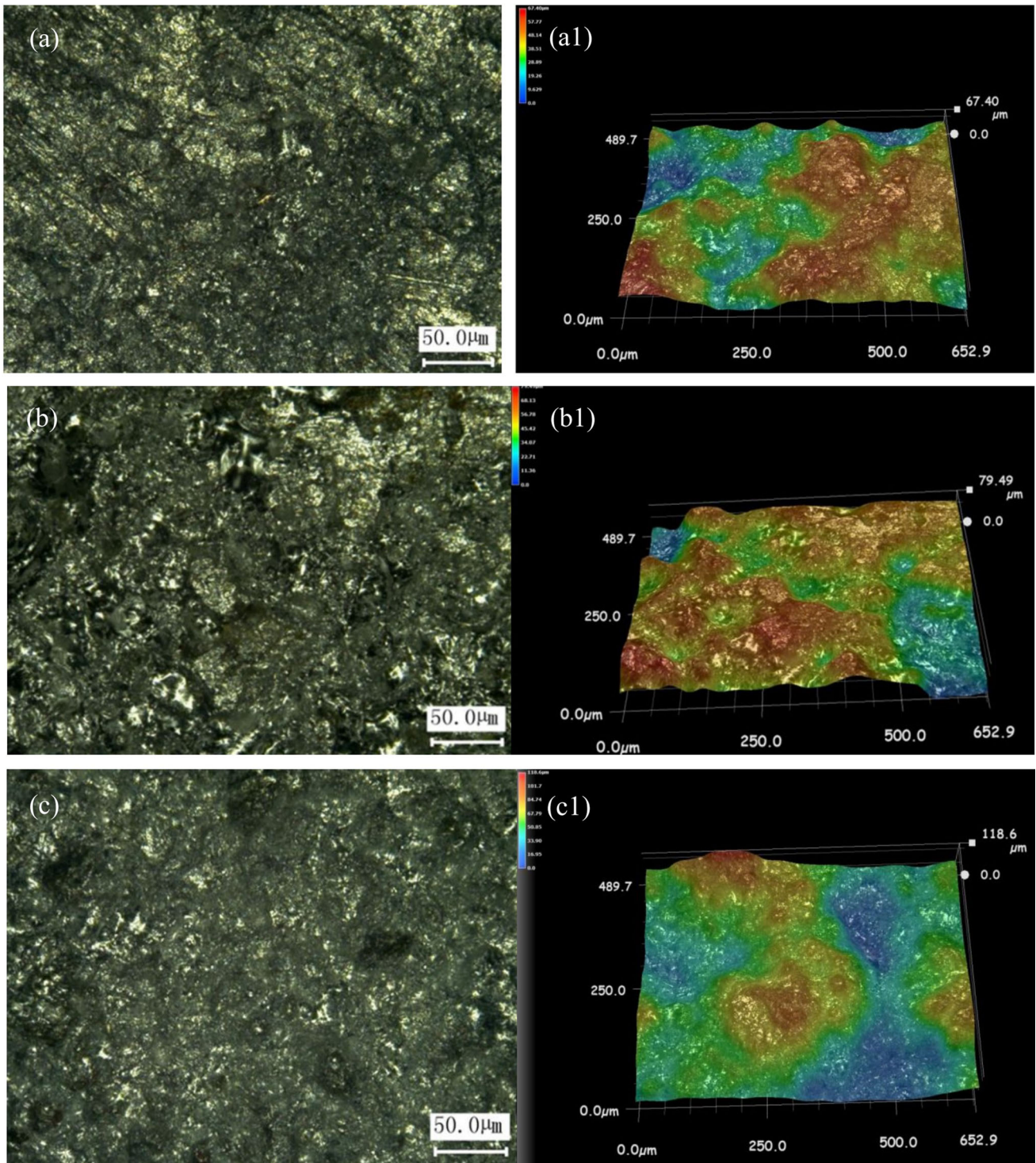


Fig. 1 Optical micrographs of 2D and 3D morphology of the top-surface of the coatings. (a) and (a1) Zn, (b) and (b1) Al, and (c) and (c1) Zn-Al coatings

of 660 °C, the particles melt and atomize unevenly during the arc-spraying process. In Fig. 1(c), Zn-Al coating was sprayed by two melted wires with different melting points and densities, and the surface of the coating was obviously undulating up to 118.6 μm. The highest peak values of Zn, Al, and Zn-Al coatings were around 67.4, 79.49, and 118.6 μm, respectively.

The surface of the coatings was relatively smooth (Fig. 1a1, b1, and c1). The surface of Zn-Al coating was rougher than that of single metallic coatings.

Figure 2 shows the SEM images and chemical composition of Zn coating. The surface of the coating was rough, and some pinholes and pores were present (Fig. 2a). In Fig. 2(a) inset of

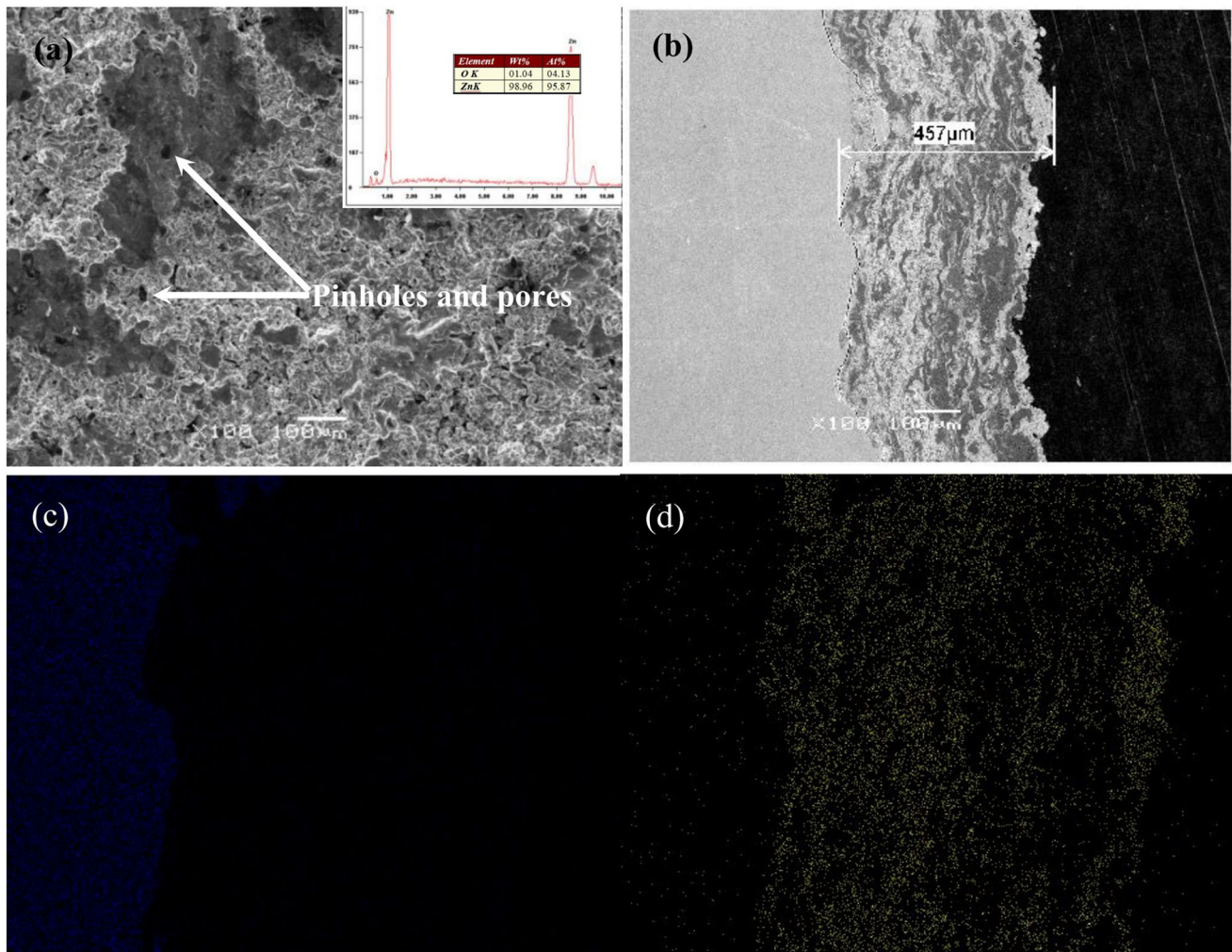


Fig. 2 SEM images of surface (a) and cross section (b) of Zn coating, (c) Fe, and (d) Zn elements

the EDS spectrum, the coating contained a certain amount of oxygen, possibly because the atomized droplets during the spraying process were oxidized by oxygen in air. There was no evidence of cracks and gaps at the interface between the substrate and the coating (Fig. 2b). The thickness of the coating was about 450 μm. The coating was a typical lamellar structure. The arc-sprayed wire was heated, accelerated, and atomized, and then the melted or semi-molten particles impacted the substrate at a high speed, cooled and solidified rapidly after flattening, and was deposited on the substrate to form the lamellar layer, and the latter sprayed material was deposited on the previous layer, thereby forming a continuous coating with a layered structure. In Fig. 2(c) and (d), the Zn element was evenly distributed in the coating. The interface between the coating and the substrate has no obvious cracks or gaps.

Figure 3 displays the SEM images and chemical composition of Al coating. The surface was also rough, and the droplets were present (Fig. 3a). A large micropore was observed on the surface. EDS spectrum proved Al coating accounted for 98.67 wt.%, a few of O-content. Al coating was distributed in the form of scales, the liquefied particles impacted the substrate. The irregular distribution of Al coating was obtained due to the effect of the substrate (Ref 40). The average thickness was about 149 μm (Fig. 3b), and there was a certain

amount of porosity. There is a zigzag mechanical combination between the coating and the substrate. The zigzag interface improved the adhesion strength due to the effect of mechanical locking. Al element was mainly distributed in the coating (Fig. 3c and d).

Figure 4 displays the morphology and chemical composition of Zn-Al coating. The surface was not smooth due to the rough surface of the substrate (Fig. 4a). The content of Zn and Al in the coating was composed of 54 at% and 46 at%, respectively, represented as Zn₅₄Al₄₆ coating. Assuming the volume of the two metal wires was the same as the sprayed Zn-Al coating was obtained under the same deposition parameters. Since the densities of Zn and Al were 7.14 and 2.7 g/cm³, respectively. It can be calculated that the mass percentage of the as-sprayed coating was Zn-73 and Al-27 wt.%, which is almost close to the result of the EDS pattern. The arc-sprayed wires become metal droplets and strike the substrate at high speed because of the action of the arc and high-pressure gas. As a result, the larger-diameter metal droplets were also liquefied before impacting the substrate. These larger-diameter semi-molten particles achieved sufficient deformation during the arc-spraying process, and finally, the large-diameter particles with a high degree of flattening were sprayed on the substrate. On the other hand, the small-diameter metal droplets cool and transform to a semi-solid state before impacting the substrate

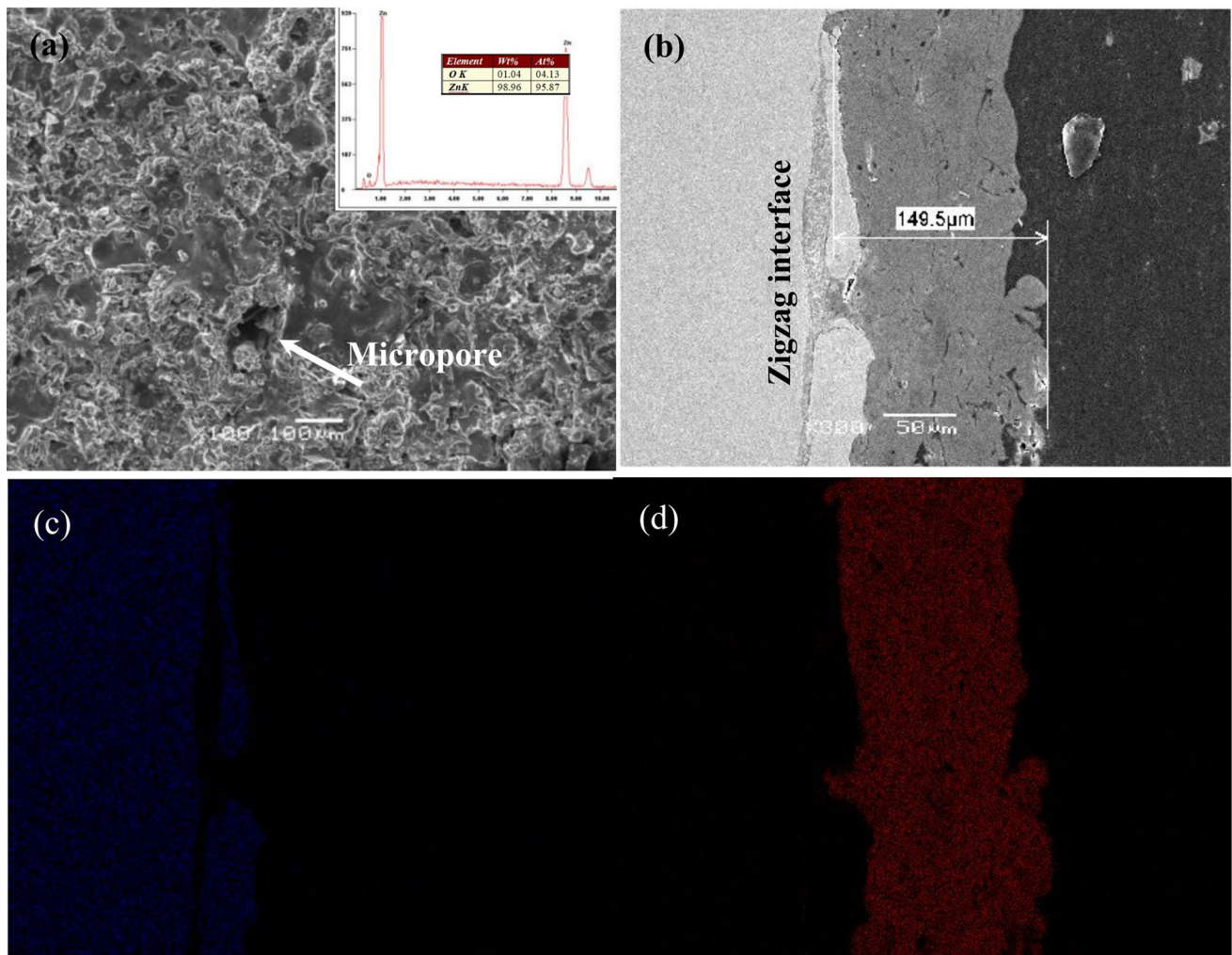


Fig. 3 SEM images of the surface (a) and cross section (b) of Al coating, (c) Fe, and (d) Al elements

surface. The deformation ability of semi-solid particles was worse than that of the liquid particles. Finally, semi-solid alloys were attached to the surface to form protrusions (Ref 41). Therefore, the coating thickness was uneven, and the average thickness was about 180 μm , and the coating exhibits an obvious lamellar structure with a few of microholes and gaps (Fig. 4b). The distribution of Zn and Al elements in the coating was relatively uniform (Fig. 4c and d), and Fe element was mainly distributed in the substrate (Fig. 4e). The porosities of Zn, Al, and Zn-Al coatings were 0.31%, 0.56%, and 0.59%, respectively. The porosity of Zn coating was lower than that of Al coating and Zn-Al coating due to the low melting point of Zn.

Figure 5 shows the XRD patterns of the coatings. There are some diffraction peaks at 36.289° , 38.99° , 43.22° , 54.32° , 70.07° , 70.63° , 77.05° , 82.08° , and 86.54° , which were corresponded to the crystal planes (002), (100), (101), (102), (103), (110), (004), (112) and (201) of Zn, indicating that the coating was composed of hexagonal Zn phase (PDF card no. # 00-87-0713), with no other impurity due to low quantity. Al coating had obvious diffraction peaks with high intensity at 38.47° , 44.72° , 65.10° , 78.23° , and 82.44° , corresponding to the crystal planes (111), (200), (220), (311), and (222), indicating that Al coating comprised a face center cubic (fcc)

structure, according to the standard Al PDF card no. #00-85-1327. The signal of Al was only detected in the XRD pattern, although Al oxide could be formed during the spraying process in air at atmospheric pressure. The oxide content in the coating might be too low to be detected. Zn-Al coating comprised Al fcc-phase and Zn hexagonal-phase. The location of the diffraction peak for Zn in the coating was the same as that of arc-sprayed Zn coating, and there was no shift. The atomic radius of Zn and Al was 1.34 \AA and 1.43 \AA , respectively. Al enters the solid solution of Zn lattice during the preparation of Zn-Al coating, and the entire unit cell of Zn becomes larger, causing the Al diffraction peak to shift toward the low Bragg angle. Therefore, some regions were just composed of Zn and Al mixture phase, the Zn-Al alloy phase may exist in the sprayed coating but was not detected by the XRD pattern.

3.2 Microhardness

From Table 2, the average microhardness values of Zn and Al single coatings, and Zn-Al coatings were 173.8 ± 18 , 181.69 ± 8.13 , and $259.88 \pm 42.19 \text{ HV}_{0.5}$, respectively. The microhardness values of cold-sprayed Zn and Al coatings were about $35 \text{ HV}_{0.1}$ (Ref 42) and $178.3 \text{ HV}_{0.1}$ (Ref 43), respectively. Kaewpradit (Ref 44) studied Zn-15Al coating had the hardness in the range of $34.86 \pm 1.95 \text{ HV}_{0.5} \sim 45.18 \pm 1.95 \text{ HV}_{0.03}$.

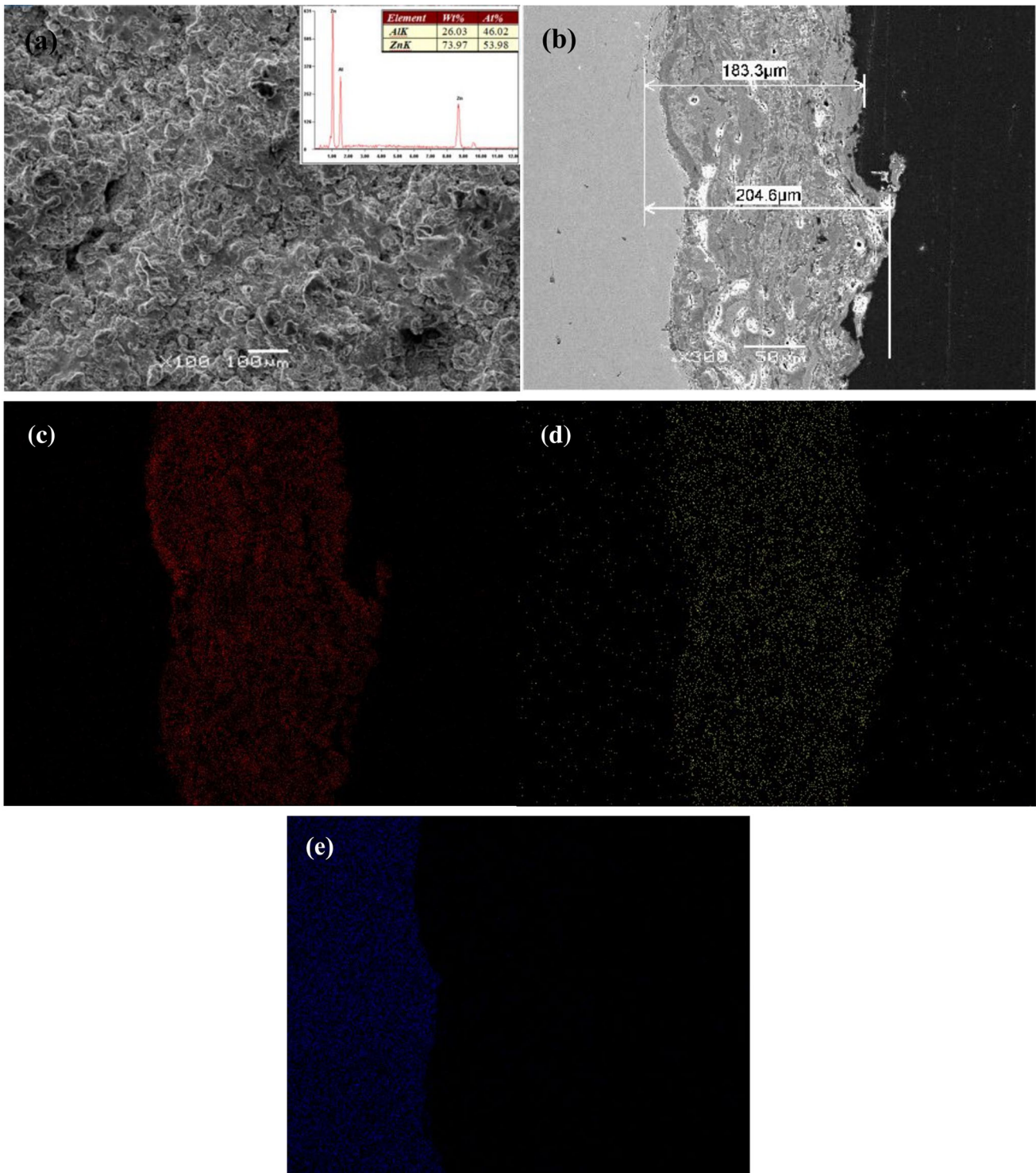


Fig. 4 SEM images of the surface (a) and cross section (b) of Zn-Al coating, (c) Al, (d) Zn, and (e) Fe elements

The mechanical properties of arc-spray coatings are highly dependent on their microstructural features. The low hardness values for the coating could be attributed to the existence of porosity, splat boundaries, and thermal stress, resulting in the reduction of microhardness (Ref 45, 46), or the volume of unwanted phases as well as the location and distribution of coating over the microstructure (Ref 39). Figure 6 shows the optical micrographs of the indentation of cross section of Zn, Al, and Zn-Al coatings. The microhardness of arc-sprayed Zn

coating was like that of Al coating, but smaller than that of Zn-Al coating. The indentation size of Zn-Al coating was smaller than that of the other coatings, indicating that the microhardness of Zn-Al coating was higher compared with arc-sprayed Zn and Al single coatings.

3.3 Abrasion Resistance

Figure 7 shows the friction coefficient curves of the coatings. The lower the coefficient of friction, the better the

wear resistance. The coefficients of friction of Al, Zn, and Zn-Al coatings were 0.7, 0.55, and 0.5, respectively. The coefficient of friction of Zn-Al coating was smaller than those of single metal coatings. Therefore, Zn-Al coating exhibited better wear resistance compared with single metallic coatings.

Figure 8 shows the optical micrographs of the morphology of the abrasion marks of the coatings. Under the same loading

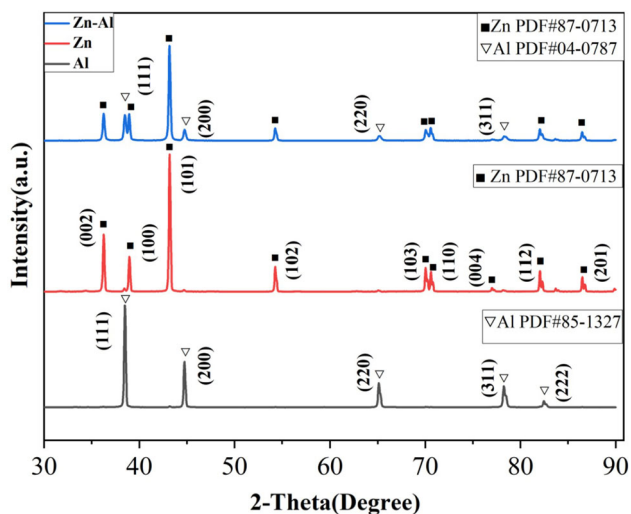


Fig. 5 XRD patterns of the coatings

and speed, there was no large amount of shedding on the surface of the coating, and there were obvious abrasion marks. The abrasion mark of Zn-Al coating (Fig. 8c) was shallower than those of single metallic coatings (Fig. 8a and b). Figure 8(a1), (b1), and (c1) shows the high-magnification optical micrographs of the wear morphology. There was metal accumulation at the edge of the wear trace, and the metal accumulation height was higher than the surface of the coating. The wear trace of Zn coating has a clear plow groove, and obvious particles (see Fig. 8a1), because the part of the abrasive chips generated by friction wear enters the friction surface, resulting in abrasive wear during the friction process. For Al coating, the wear trace has a deep groove and some particles (Fig. 8b1). The coating was seriously worn in the middle of the wear trace. For Zn-Al coating, the morphology of the wear trace was composed of shallow depth, and some adhesive wear pits (Fig. 8c1). Al with an fcc structure has good toughness, and Al coating is prone to plastic deformation when adhesion wear occurs. Therefore, the shear fracture of the adhesion occurs, and then the wear debris is formed (Ref 20, 47). Zn with a close-packed hexagonal structure is not prone to plastic deformation under external loading. The adhesive wear of Zn-Al coating is slight, so the tendency of Zn-Al coating to undergo adhesive wear is dependent on the content of the Al phase in the coating.

Figure 9 shows the optical micrographs of the 3D morphology of the scratches of the coatings after wear test. The width and depth of scratches of Zn (Fig. 9a) and Al coatings (Fig. 9b) were more obvious than those of Zn-Al coating (Fig. 9c).

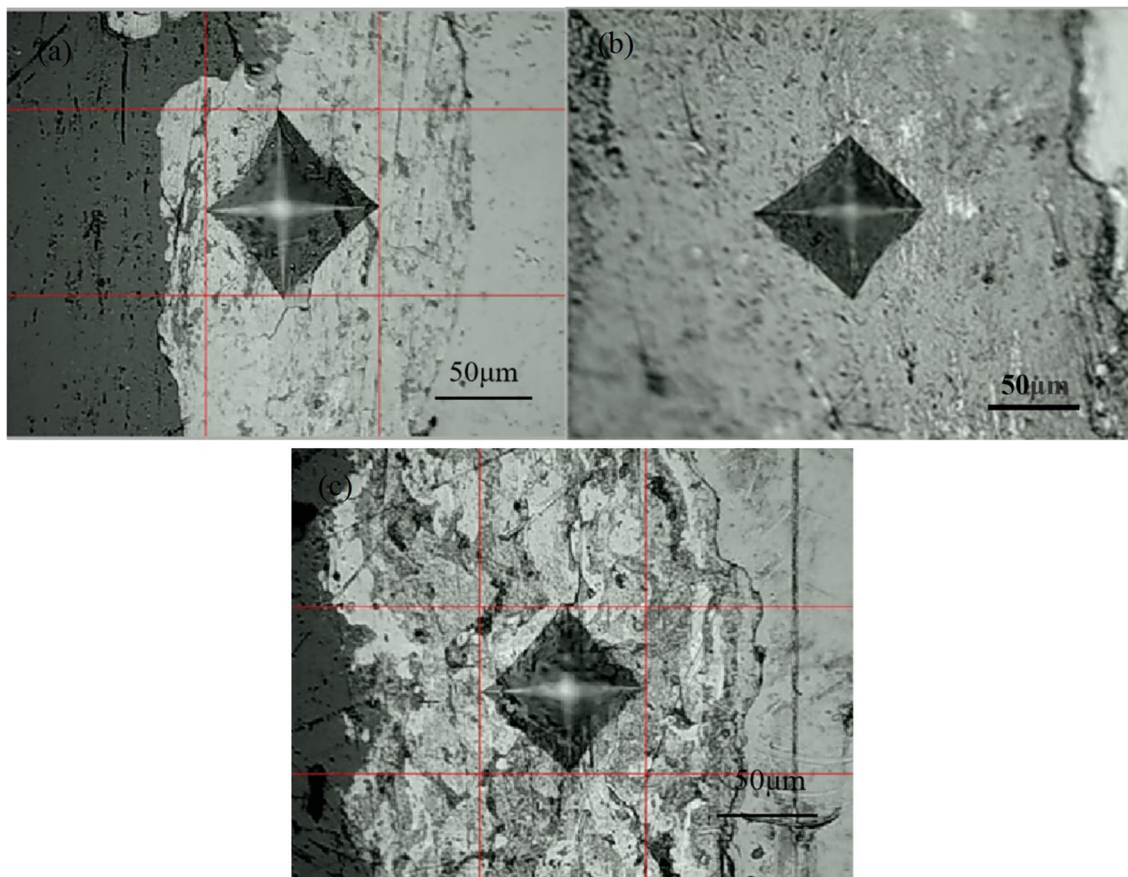


Fig. 6 Optical micrographs of indentation of cross section of (a) Zn, (b) Al, and (c) Zn-Al coatings

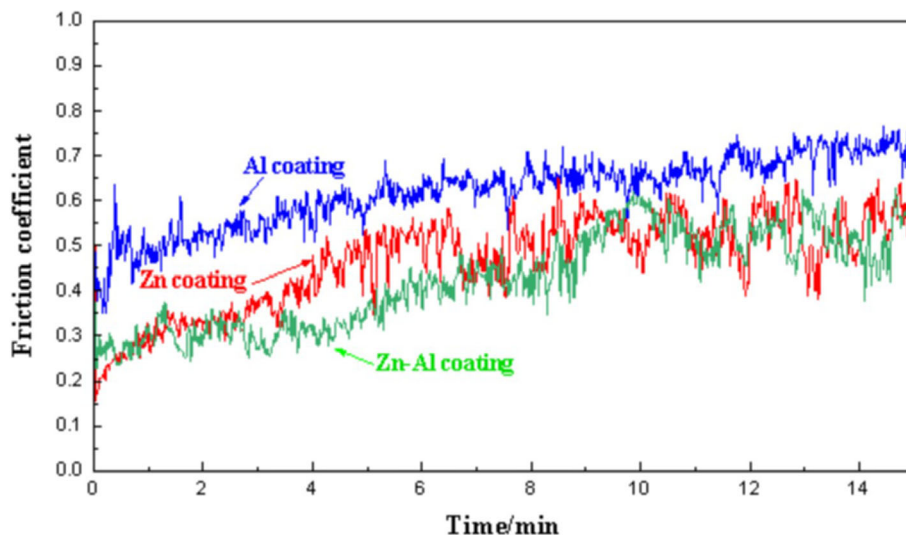


Fig. 7 Friction coefficient plots of the coatings after the wear test

Figure 10 displays the contour plots of the middle portion of the wear trace. The width and depth of Zn-Al coating were $241.9 \mu\text{m}$ and $24.41 \mu\text{m}$, respectively, which were lower than those of Zn and Al single metallic coatings. Zn-Al coating has better wear resistance compared with single metallic coatings because Zn-Al coating was mechanically mixed with Zn, Al, and a small number of alloys.

3.4 Electrochemical Corrosion Resistance

Figure 11 shows the OCP curves against the testing time for the coatings. The OCP values of Zn, Al, and Zn-Al coatings were about -1.01 , -1.00 , -1.06 V, respectively. The OCP curve of Zn-Al coating was first stable, then changed to a much more negative value, and kept stable. Just considering the OCP value, the anticorrosion performance of the coating was sorted in the order of $\text{Al} > \text{Zn} > \text{Zn-Al}$.

Tafel polarization curves of the coatings are shown in Fig. 12. Table 2 lists the electrochemical corrosion data of the coatings, including the corrosion potential (E_{corr}) and corrosion current density (I_{corr}). The corrosion potential values of Al, Zn, and Zn-Al coatings were -1.08 , -1.31 , and -2.98 V, respectively. In general, the coatings have a high E_{corr} and low I_{corr} values, indicating the chemical stability was good, and the corrosion rate was low (Ref 41). In Fig. 12(a), (b), and (c), the corrosion potential of Zn-Al coating was always lower than those of single metallic coatings. The corrosion potential of Zn-Al coating was the lowest, about -2.985 V, and its ability to protect the cathode as a sacrificial anode was the strongest. The corrosion current density of Zn-Al coating was almost close to Al coating, but both are larger than Zn coating, because of the passive film ($\text{Al}(\text{OH})_3$ or Al_2O_3) on the surface of Al coating after polarization test. The passive film could limit the penetration of the corrosive medium and be acted as an excellent barrier layer. Zn54Al46 coating contains rich Zn, which could influence the corrosion resistance of the coating. Therefore, the corrosion current density of Zn54Al46 coating was slightly less than that of Al coating. However, the polarization resistance value of Zn54Al46 coating is the largest, compared with a single metallic coating. The polarization resistance value of the coating was high, and the anti-corrosion performance is good. Therefore, taking all factors into consid-

eration, Zn54Al46 coating exhibited better corrosion resistance than single metallic coatings of Zn and Al.

Figure 13 shows the electrochemical impedance spectra of the coatings. In Fig. 13(a), the semicircle of Al coating was larger than that of Zn coating. The impedance arc radius of Zn-Al coating was significantly larger than those of the single metallic coatings, indicating that Zn-Al coating has better corrosion resistance compared with single metallic coatings (Ref 48). The electrochemical impedance spectra of Zn and Al coatings were composed of one large semicircle and one small arc radius, however, Zn-Al coating has just one large semicircle. Therefore, the electrochemical corrosion mechanisms of single metal coating and Zn-Al coating were different, discussing this issue below.

The Bode plots are present in Fig. 13(b) and (c). The impedance modulus values were almost stable at the low-frequency range (Fig. 13b). However, the modulus of Zn-Al coating was higher than that of single coatings at the low-frequency stage, indicating the anti-corrosion performance of the coatings was taken in the order of $\text{Zn-Al} > \text{Al} > \text{Zn}$. Although the thickness of Zn coating was the largest, Zn coating exhibited poor corrosion resistance. In Fig. 13(b), there was a high broad peak for Zn and Al coatings at 41.4 and 49.5° respectively. However, the phase plot of Zn-Al coating was not stable, but the phase angle of the coating was relatively higher than those of single metallic coatings, indicating better corrosion resistance.

The equivalent circuit diagrams of the three coatings are shown in Fig. 13(d). The equivalent circuit of Zn-Al coating is $\text{R}(\text{QR})$ type, where R_s was the solution resistance, and R_t and CPE_b represented the charge transfer resistance and the capacitance at the interface between the solution and the substrate, respectively. However, the equivalent circuit of single metallic coating is $\text{R}(\text{Q}(\text{R}(\text{QR})))$ type, where R_b and CPE_b were the resistance and capacitance of the passive layer respectively, and R_t and CPE_t were the charge transfer resistance and capacitance respectively (Ref 40). Table 3 displays the electrochemical impedance data of the simulated equivalent circuit. According to the above data, Zn-Al coating has good anticorrosion performance due to high corrosion potential and high width of the capacitive loop (Ref 49).

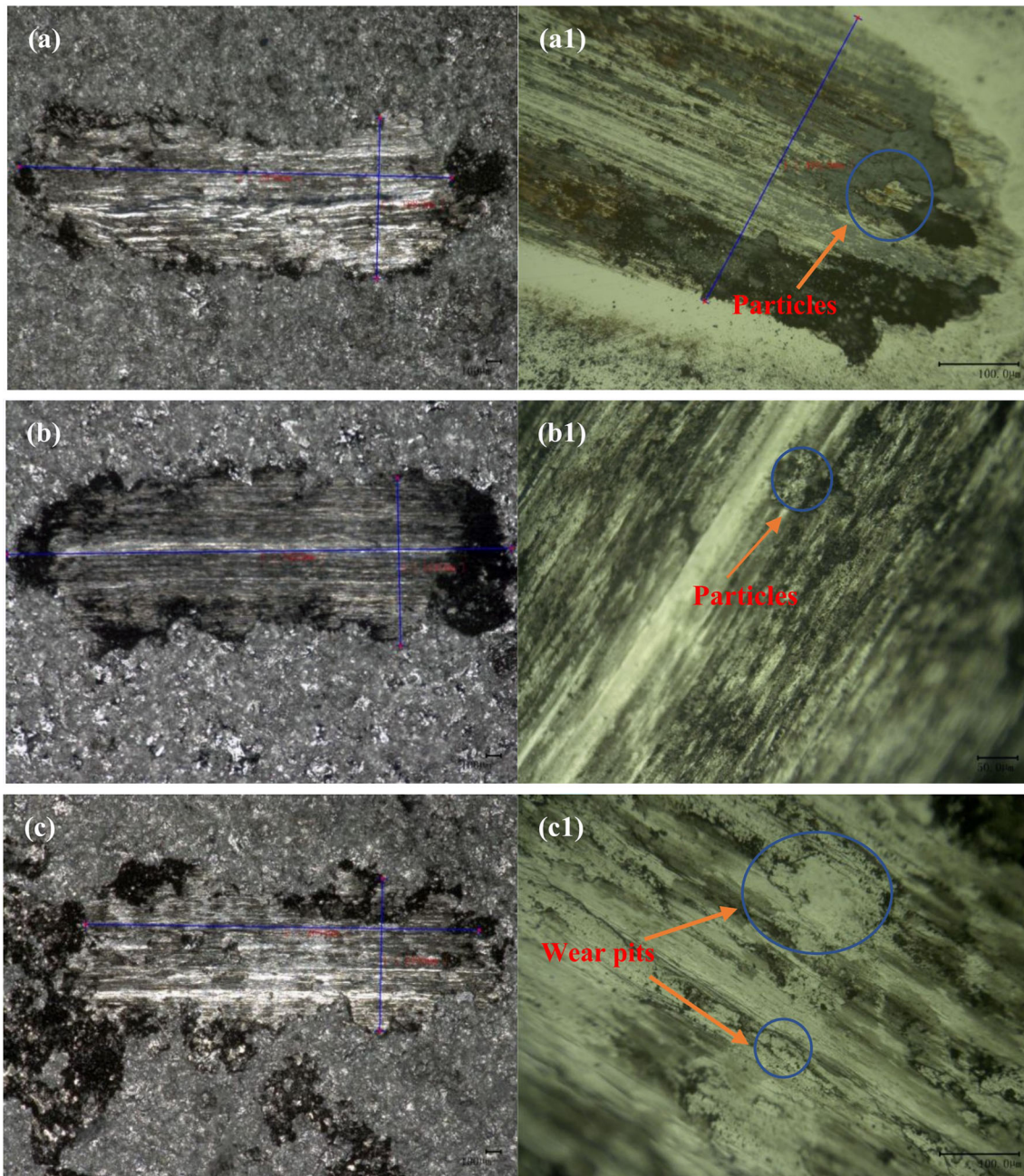


Fig. 8 Optical micrographs of wear trace of Zn (a) and (a1), Al (b) and (b1), Zn-Al (c) and (c1) coatings after wear test

The surface of Al coating was off-white, and corrosion products were formed on the surface of the coating. In the presence of Cl^- in solution, the dense oxide film on the surface of Al coating is destroyed, the coating was further eroded due to the large porosity of Al coating, and the corrosion product was flocculent $\text{Al}(\text{OH})_3$, which was not easy to dissolve in the NaCl solution (Ref 40). The passive film had a good sealing effect on the porosity, the corrosion product forms an effective barrier on the coating, the corrosion resistance was greatly improved, and the corrosion rate was significantly reduced. The surface of Zn coating was blue-gray, and the surface was covered with white corrosion products. At the beginning of the corrosion, due to the rapid penetration of the corrosion medium with micro defects in the coating, the coating was corroded and oxidized to form an oxide layer, namely ZnO. The corrosion

products are not easy to diffuse, and the sealing effect is weak. Zn has a cathodic protection effect on steel, Zn coating was sacrificially corroded, while the base is not affected. The anti-corrosion performance of Zn coating depends mainly on its thickness and microstructure. During the corrosion process, the spots with different sizes appear on the surface of Zn-Al coating. There were many white corrosion products, and the corrosion substances are delicate and loose, which were easy to peel off. The corrosion products of the coating are mainly granular, which was similar to the microscopic corrosion form of Zn coating. When the corrosion occurred, the uneven corrosive phenomena occurred in the coating due to the rich-Zn in the Zn-Al coating. The Zn-rich phase was preferentially dissolved, the corrosion products of Zn were attached to the surface of Al coating. The phase distribution on the surface was

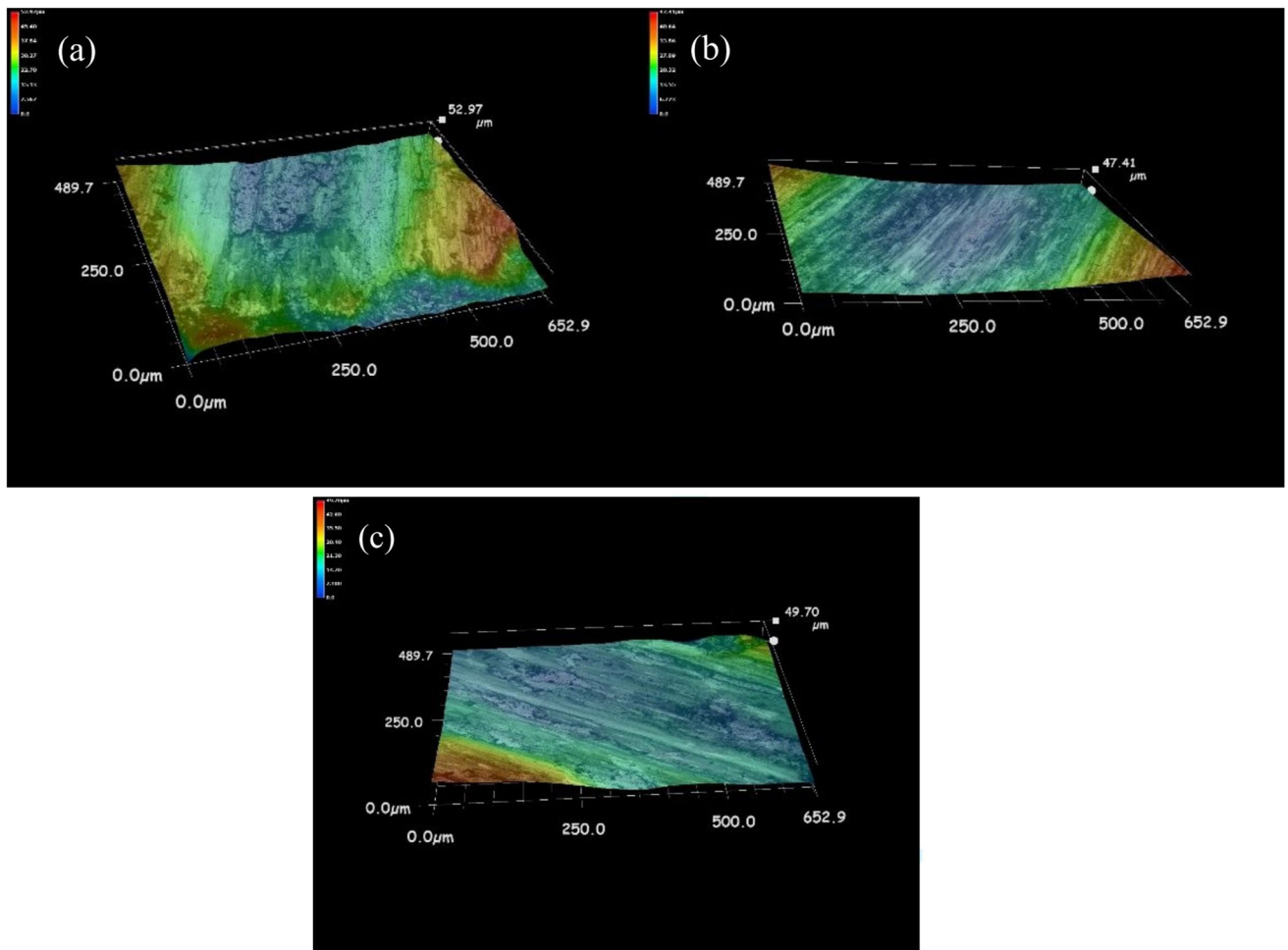


Fig. 9 3D morphology photos of scratches of the coatings after wear test. Zn (a), Al (b), and Zn-Al (c) coatings

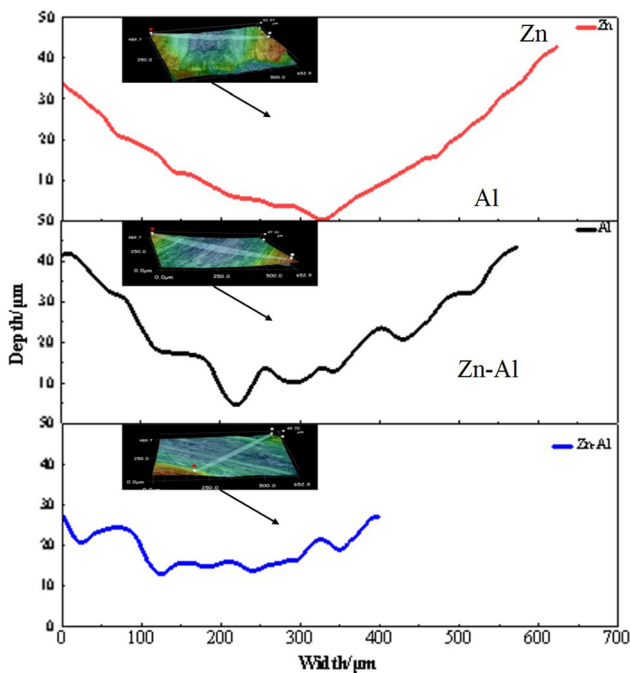


Fig. 10 The contour plots of the middle portion of the wear trace

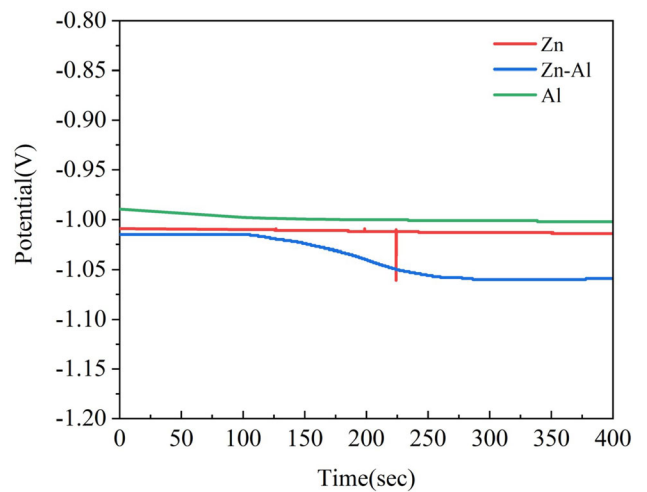


Fig. 11 OCP curves vs. testing time for the coatings

uneven, the gaps were formed due to the preferential dissolution of Zn-rich phase. The Zn-Al coating combined the passive behavior of Al and the sacrifice of anodic protection of Zn (Ref 24). The thickness of Zn-rich and Al-rich phase layers was limited, so as the Zn phase dissolved, Al and Zn-Al alloy phases fell off. The white rust on the surface of Zn-Al coating is

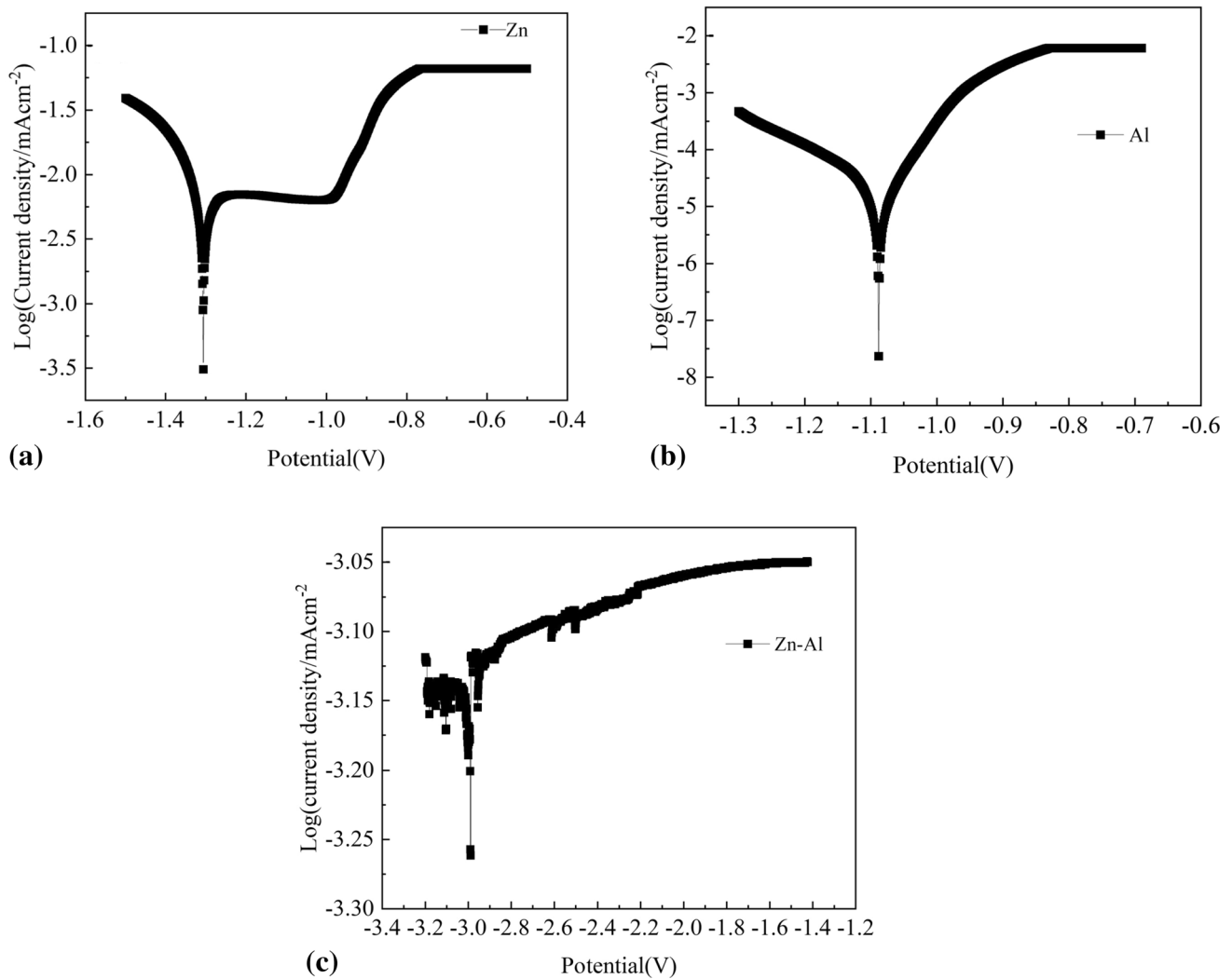


Fig. 12 Polarization curves of (a) Zn, (b) Al, and (c) Zn-Al coatings

mainly composed of ZnO and Zn(OH)₂, containing a small amount of oxides Al₂O₃ and Al(OH)₃. The chemical reaction formula for the cathode is written as follows:



4. Conclusions

Zn-Al, Zn, and Al coatings were sprayed on the carbon steel by arc spraying technology. The microstructure, phase identification, chemical composition, hardness, wear, and corrosion

resistance of the coatings were studied in detail. There are some main conclusions as follows:

- (1) The average thickness of Zn-Al, Zn, and Al coatings was about 183, 450, and 149 μm , respectively. The coatings had a lamellar structure, with no evidence of delamination and cracking. Zn coating was composed of Zn and a few quantities of oxide. Al coating comprised Al and Al₂O₃ phases. Zn-Al coating was composed of Al and Zn phases, and a few of Zn-Al alloys.
- (2) The average microhardness of Zn-Al, Zn, and Al coatings was about 259.88HV, 173.8HV, and 181.69HV, respectively. The hardness of Zn-Al coatings was higher than that of single metallic coatings.
- (3) The friction coefficients of Zn-Al, Zn, and Al coatings were 0.5, 0.55, and 0.7, respectively. The wear resistance of Zn-Al coating was better than that of Zn and Al coatings.
- (4) The anti-corrosion performance of Zn-Al coating was better than that of the single metallic coatings. Zn-Al coating had the smallest E_{corr} value of about -2.985 V , indicating that the ability of Zn-Al coating to protect the cathode as a sacrificial anode was good.

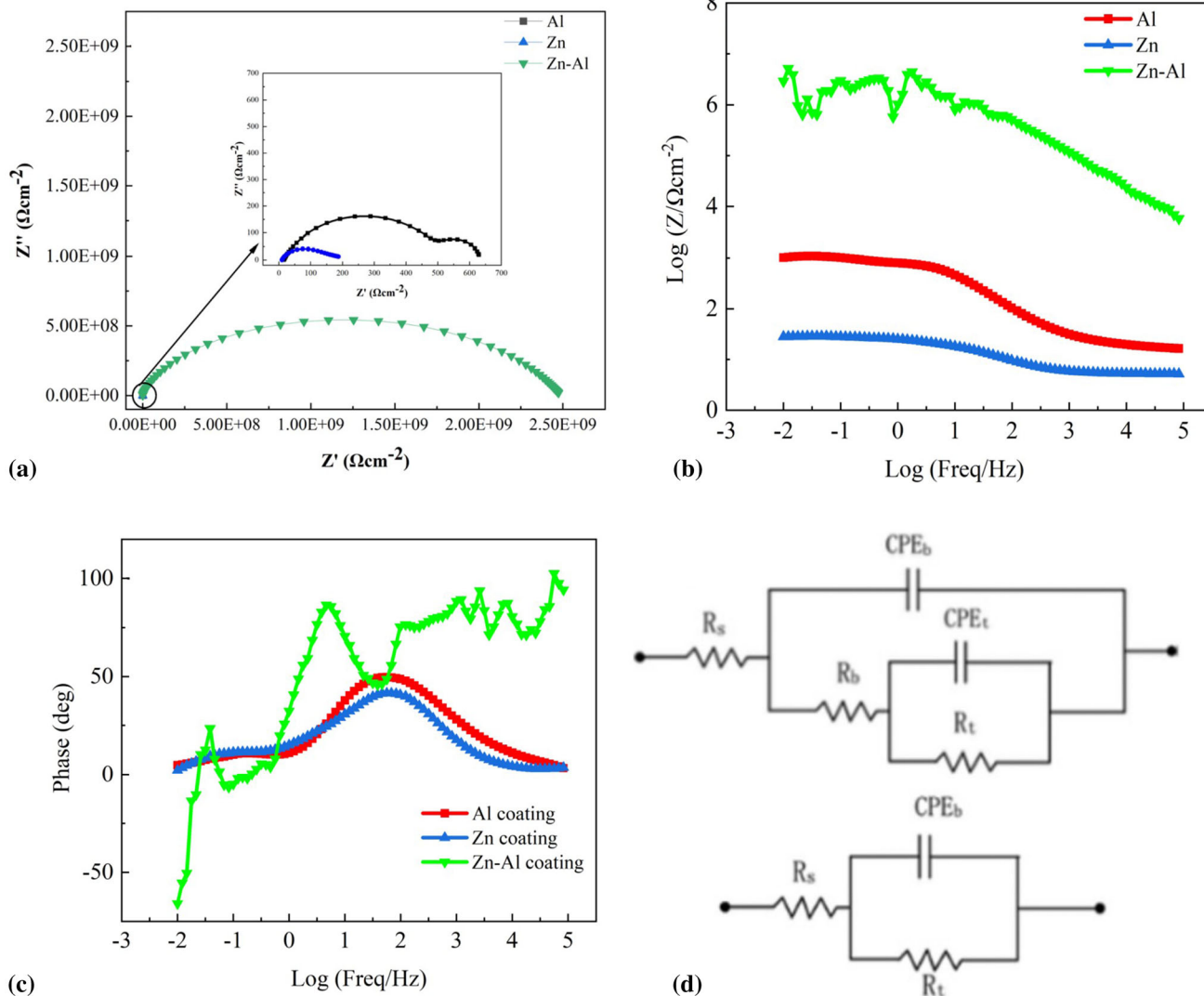


Fig. 13 Electrochemical impedance spectra of the coatings (a) Nyquist diagram, (b) Frequency-phase Bode diagram, (c) Frequency-impedance modulus Bode diagram, and (d) Fitted circuit diagram of Zn and Al coating (upper), and Zn-Al coating (below)

Table 3 Electrochemical corrosion data

Coating	E_{ocp} , V	E_{corr} , V	I_{corr} , Acm^{-2}	R_p , Ωcm^{-2}
Al	-1.00	-1.08	5.36×10^{-5}	405.6
Zn	-1.01	-1.31	5.37×10^{-4}	117.5
Zn-Al	-1.06	-2.98	5.64×10^{-5}	1593

Table 4 Impedance fitted circuit data

Coating	R_s , Ωcm^2	R_b , Ωcm^2	R_t , Ωcm^2	CPE_b	CPE_t
Zn	18.06	101.6	154.9	$3.69E-5$	$3.38E-4$
Al	14.95	63.82	393.6	$1.34E-5$	$3.94E-5$
Zn-Al	$2.61E4$	-	$1.98E9$	$1.71E-6$	-

Acknowledgments

The authors thank Mr. Guang Yang from the Analysis and Testing Center, NERC Biomass of Changzhou University for the discussion and for helping in the XRD measurement, respectively.

References

1. B.R. Hou, *Ocean Environment Corrosion Theory and Its Application*, 1st ed., B. Peng Ed., Science Press, Beijing, 1999, p 199
2. Y. Bai and Q. Bai, *Subsea Pipelines and Risers*, 2nd ed. Elsevier Science Ltd., Amsterdam, 2005, p 229
3. K.L. Money, *Corrosion Testing in the Atmosphere*, *Metals Handbook*, 9th ed. ASM International, Materials Park, 1987, p 49
4. D.P. Schmidt, B.A. Shaw, E. Sikora, W.W. Shaw, and L.H. Laliberte, Corrosion Protection Assessment of Sacrificial Coating Systems as a Function of Exposure Time in a Marine Environment, *Prog. Org. Coat.*, 2006, **57**(4), p 352–364.
5. J. Huang, Y. Liu, J. Yuan, and H. Li, Al/Al₂O₃ Composite Coating Deposited by Flame Spraying for Marine Applications: Alumina

- Skeleton Enhances Anti-corrosion and Wear Performances, *J. Therm. Spray. Tech.*, 2014, **23**, p 676–683.
6. J. Kawakita, T. Fukushima, S. Kuroda, and T. Kodama, Corrosion Behaviour of HVOF Sprayed SUS316L Stainless Steel in Seawater, *Corros. Sci.*, 2002, **44**(11), p 2561–2581.
 7. H.B. Choe, H.S. Lee, M.A. Ismail, and M.W. Hussin, Evaluation of Electrochemical Impedance Properties of Anti-corrosion Films by Arc Thermal Metal Spraying Method, *Int. J. Electrochem. Sci.*, 2015, **10**(11), p 9775–9789.
 8. F. Ahnia and B. Demri, Evaluation of Aluminum Coatings in Simulated Marine Environment, *Surf. Coat. Technol.*, 2013, **220**, p 232–236.
 9. D. Chaliampalias, G. Vourlias, E. Pavlidou, G. Stergioudis, S. Skolianos, and K. Chrissafis, High Temperature Oxidation and Corrosion in Marine Environments of Thermal Spray Deposited Coatings, *Appl. Surf. Sci.*, 2008, **255**(5), p 3104–3111.
 10. L.J. Fang, J. Huang, Y. Liu, B.T. Zhang, and H. Li, Cored-wire Arc Spray Fabrication of Novel Aluminium-Copper Coatings for Anti-Corrosion/Fouling Hybrid Performances, *Surf. Coat. Technol.*, 2019, **357**, p 794–801.
 11. M. Hauer, K.M. Henkel, S. Krebs, and W. Kroemmer, Alternative Gas Mixtures in Arc Spraying: A Chance to Improve Coating Properties and Residual Stress States, *J. Therm. Spray. Tech.*, 2018, **27**, p 106–118.
 12. D.J. Kong, X.Q. Dong, and J.C. Wang, Effects of Anodic Oxidation on Corrosion Properties of Al Coating by Arc Spraying in Seawater, *Surf. Interf. Anal.*, 2015, **47**(9), p 911–918.
 13. J.R. Lin, Z.H. Wang, P.H. Lin, J.B. Cheng, X. Zhang, and S. Hong, Microstructure and Cavitation Erosion Behavior of FeNiCrBSiNbW Coating Prepared by Twin Wires Arc Spraying Process, *Surf. Coat. Technol.*, 2014, **240**, p 432–436.
 14. V. Geamăn, M.A. Pop, I. Radomir, and D.L. Motoc, Ni-5Al-Cladding by Thermal Arc Spraying, *Int. J. Modern Manuf. Technol.*, 2014, **6**, p 55–58.
 15. A. Gulec, O. Cevher, A. Turk, F. Ustel, and F. Yilmaz, Accelerated Corrosion Behaviors of Zn, Al and Zn/15Al Coatings on a Steel Surface, *Mater. Technol.*, 2011, **45**(5), p 477–482.
 16. D. Rincón, A. Rincón, M. Sanchez, N. Romero, O. Salas, R. Delgado, B. Lopez, J. Uruchurtu, M. Marroco, and Z. Panosian, Evaluating Zn, Al and Al-Zn Coatings on Carbon Steel in a Special Atmosphere, *Constr. Build. Mater.*, 2009, **23**, p 1465–1471.
 17. B. Song, S.J. Dong, H.I. Liao, and C. Coddet, Microstructure and wear resistance of FeAl/Al₂O₃ intermetallic, *Surf. Coat. Technol.*, 2015, **268**, p 24–29.
 18. A.R.M. Sahab, N.H. Saad, S. Kasolang, and J. Saedon, Impact of Plasma Spray Variables Parameters on Mechanical and Wear Behavior of Plasma Sprayed Al₂O₃+3wt.% TiO₂ Coating in Abra-Sion and Erosion Application, *Int. Symp. Robot Intell. Sens.*, 2012, **41**, p 1689–1695.
 19. J. Huang, Y. Liu, J.H. Yuan, and H. Li, Al-Al₂O₃ Composite Coating Deposited by Flame Spraying for Marine Applications: Alumina Skeleton Enhances Anti-corrosion and Wear Performances, *J. Therm. Spray. Technol.*, 2014, **23**, p 676–683.
 20. W.G. Chen, Z.X. Wang, G.L. Xu, W.T. Song, Y. Xie, L. Zhao, M.H. Xia, and W. Li, Friction and Anti-corrosion Characteristics of Arc Sprayed Al+Zn Coatings on Steel Structures Prepared in Atmospheric Environment, *J. Mater. Res. Technol.*, 2021, **15**, p 6562–6573.
 21. A. Pritzel Dos Santos, S.M. Manhobosco, J.S. Rodrigues, and L.F.P. Dick, Comparative Study of the Corrosion Behavior of Galvanized, Galvannealed and Zn55Al Coated Interstitial Free Steels, *Surf. Coat. Tech.*, 2015, **279**, p 150–160.
 22. X.X. Liu and D.J. Kong, Salt Spray Corrosion and Electrochemical Corrosion Performances of Dacromet Fabricated Zn–Al Coating, *Anti-Corrosion Methods and Materials*, 2019, **66**, p 565–572.
 23. K. Tachibana, Y. Morinaga, and M. Mayuzumi, Hot Dip Fine Zn and Zn–Al Alloy Double Coating for Corrosion Resistance at Coastal Area, *Corros. Sci.*, 2007, **49**(1), p 149–157.
 24. M. Morcillo, E. Palma, and B. Fernandez, Atmospheric Galvanic Protection of 55% Al-Zn Precoated Steel, *Mater. Corros.*, 1994, **45**, p 550–553.
 25. T. Prosek, D. Persson, J. Stoullil, and D. Thierry, Composition of Corrosion Products Formed on Zn-Mg, Zn-Al and Zn-Al-Mg Coatings in Model Atmospheric Conditions, *Corros. Sci.*, 2014, **86**, p 231–238.
 26. S. Schürz, G.H. Luckeneder, M. Fleischanderl, P. Mack, H. Gsaller, A.C. Kneissl, and G. Mori, Chemistry of Corrosion Products on Zn-Al-Mg Alloy Coated Steel, *Corros. Sci.*, 2010, **52**(10), p 3271–3279.
 27. Q. Jiang, Q. Miao, W.W. Liang, F.G. Ying, F. Tong, Y. Xu, B.L. Ren, Z.J. Yao, and P.Z. Zhang, Corrosion Behavior of Arc Sprayed Al-Zn-Si-RE Coatings on Mild Steel in 3.5 wt.% NaCl Solution, *Corros. Sci.*, 2014, **86**, p 644–656.
 28. D.X. Fu, B.S. Xu, W. Zhang, S.C. Wei, and Y. Liu, Failure Mechanism of Organic Coatings Overlaid on Arc Sprayed Coatings, *Surf. Eng.*, 2009, **25**(8), p 612–614.
 29. S. Djerourou, H. Lahmar, N. Bouhellal, and Y. Mebdoua, Study of Twin Wire Arc Sprayed Zinc/Aluminum Coating on Low Carbon Steel Substrate: Application to Corrosion Protection, *Adv. Mater. Res.*, 2013, **685**, p 271–276.
 30. W. Kroemmer, High performance arc sprayed coatings for active corrosion protection in offshore applications, in *Proceedings of the International Thermal Spray Conference*, 2013, p. 97
 31. W.M. Zhao, Y. Wang, C. Liu, L.X. Dong, H.H. Yu, and H. Ai, Erosion-Corrosion of Thermally Sprayed Coatings in Simulated Splash Zone, *Surf. Coat. Technol.*, 2010, **205**(7), p 2267–2272.
 32. J.H. Kim and M.H. Lee, A Study on Cavitation Erosion and Corrosion Behavior of Al⁺, Zn⁺, Cu⁺, and Fe-based Coatings Prepared by Arc Spraying, *J. Therm. Spray Technol.*, 2010, **19**, p 1224–1230.
 33. S. Hong, Y. Wu, W. Gao, J. Zhang, and Y. Qin, Corrosion Behavior of Arc-Sprayed Zn-Al Coating in the Presence of Sulfate-Reducing Bacteria in Seawater, *J. Mater. Eng. Perform.*, 2015, **24**, p 4449–4455.
 34. Z.X. Zhu, B.X. Xu, and Y.X. Chen, Effect of Al Content on Electrochemical Corrosion Behavior of Arc Sprayed Zn-Al Coating, *China Surf. Eng.*, 2011, **24**, p 58–61. (in Chinese)
 35. B. Lin and L.L. Li, Electrochemical Corrosion Behavior of Arc Sprayed Zn and Zn15Al Coatings in Simulated Salina Soil and Neutral Meadow Soil Solutions, *J. Wuhan Univer. Technol. Mater. Sci. Edit.*, 2011, **26**, p 1152–1156.
 36. S.F. Bonabi, F. Ashrafzadeh, A. Sanati, and S.M. Nahvi, Structure and Corrosion Behavior of Arc-Sprayed Zn-Al Coatings on Ductile Iron Substrate, *J. Therm. Spray Technol.*, 2018, **27**, p 524–537.
 37. B. Shaw and P.J. Moran, Characterization of the Corrosion Behavior of Zinc-Aluminum Thermal Spray Coatings, *Mater. Perform.*, 1985, **24**, p 22–31.
 38. T.C. Chen, C.C. Chou, T.Y. Yung, K.C. Tsai, and J.Y. Huang, Wear Behavior of Thermally Sprayed Zn/15Al, Al and Inconel 625 Coatings on Carbon Steel, *Surf. Coat. Technol.*, 2016, **303**(Part A), p 78–85.
 39. A. Darabi and F. Azarmi, Investigation on Relationship Between Microstructural Characteristics and Mechanical Properties of Wire-Arc-Sprayed Zn-Al Coating, *J. Therm. Spray Technol.*, 2020, **29**, p 297–307.
 40. P. Li, X. Huang and D.J. Kong, Corrosive Wear and Electrochemical Corrosion Performances of Arc Sprayed Al Coating in 3.5% NaCl Solution, *Anti-Corros. Methods Mater.*, 2021, **68**, p 95–104.
 41. S. Feng, L. Jia, H. Zhang, F. Wang, G. Liu, and H. Zhang, Corrosion Behaviour of Arc Sprayed Zn55Al Coatings on Q235 Steel in 3.5 wt.% NaCl Solution, *Rare Metal Mater. Eng.*, 2019, **48**, p 1087–1095.
 42. N.B. Maledi, O.P. Oladijo, I. Botef, T.P. Ntsoane, A. Madiseng, and L. Moloisane, Influence of Cold Spray Parameters on the Microstructures and Residual Stress of Zn Coatings Sprayed on Mild Steel, *Surf. Coat. Technol.*, 2017, **318**, p 106–113.
 43. Y. L. Liu, X.L. Li, Q. Zhang, and C.H. Xu, Study on microstructure and mechanical properties of cold spraying Al coating on magnesium alloy, in *Proceedings of the 2015 International Power, Electronics and Materials Engineering Conference*, 2015
 44. T. Kaewpradit, D. Yutthakamthon, W. Pongsaksawad, P. Sheppard, H. Koiprasert, and C. Banjongprasert, Microstructure and Properties of Arc Sprayed Zn-Al Alloy Coatings, *J. Physics: Conf. Series*, 2021, **1719**, p 012113.
 45. A. Darabi and F. Azarmi, Investigation on Relationship Between Microstructural Characteristics and Mechanical Properties of Wire-Arc-Sprayed Zn-Al Coating, *J. Therm. Spray. Technol.*, 2020, **29**, p 297–307.
 46. D. Chicot, H. Ageorges, M. Voda, G. Louis, M.A. Ben Dhia, C.C. Palacio, and S. Kossman, Hardness of thermal sprayed coatings: relevance of the scale of measurement, *Surf. Coat. Technol.*, 2015, **268**, p 173–179.

47. X.X. Luo, Preparation of Fe-Al based laser cladding coating and its toughening and anti-wearing mechanism, Nanjing University of Aeronautics and Astronautics, 2018, 1, in Chinese
48. W.P. Wu and J.J. Jiang, Effect of Plating Temperature on Electroless Amorphous Ni-P film on Si Wafers in an Alkaline Bath Solution, *Appl. Nanosci.*, 2017, 7, p 325–333.
49. W.P. Wu, J.W. Liu, Y. Zhang, and X. Wang, Electrochemical Characteristics of Iridium Coating by Double Glow Plasma Discharge Process on Titanium Alloy Substrates, *Surf. Eng.*, 2019, 35(11), p 954–961.

Publisher's Note Springer Nature remains neutral with regard to jurisdictional claims in published maps and institutional affiliations.

Springer Nature or its licensor (e.g. a society or other partner) holds exclusive rights to this article under a publishing agreement with the author(s) or other rightsholder(s); author self-archiving of the accepted manuscript version of this article is solely governed by the terms of such publishing agreement and applicable law.